The Last Deglaciation Event in the Eastern Central Arctic Ocean

Ruediger Stein, Seung-Il Nam, Carsten Schubert, Christoph Vogt, Dieter Fütterer, Jan Heinemeier

Oxygen isotope records of cores from the central Arctic Ocean yield evidence for a major influx of meltwater at the beginning of the last deglaciation 15.7 thousand years ago (16,650 calendar years B.C.). The almost parallel trends of the isotope records from the Arctic Ocean, the Fram Strait, and the east Greenland continental margin suggest contemporaneous variations of the Eurasian Arctic and Greenland (Laurentide) ice sheets or increased export of low-saline waters from the Arctic within the East Greenland Current during the last deglaciation. On the basis of isotope and carbon data, the modern surface- and deep-water characteristics and seasonally open-ice conditions with increased surface-water productivity were established in the central Arctic at the end of Termination Ib (about 7.2 thousand years ago or 6,000 calendar years B.C.).

In low and mid-latitudes as well as subpolar regions, accelerator mass spectrometry (AMS)^{14}C-dated, high-resolution stable oxygen isotope records are well established for Quaternary chronostratigraphy and are used for detailed reconstructions of the Northern Hemisphere glaciation history (*1–7*). Such records, on the other hand, are very rare for the Arctic Ocean (*8–10*) and even unavailable until now for the most interior areas of the Arctic, such as the Lomonosov Ridge and the Amundsen Basin. Because of the lack of satisfactory stable isotope data, the detailed late Quaternary chronostratigraphic framework as well as paleoceanographic reconstructions in the central Arctic Ocean and their significance for the global climate system are still controversial (*11–15*). We present AMS^{14}C-dated isotope and carbon records that may help solve some of these controversies.

During the ARCTIC '91 expedition to the eastern central Arctic Ocean, sediment cores were recovered from the Nansen, Amundsen, and Makarov basins, the Gakkel and Lomonosov ridges, the Morris-Jesup Rise, and the Yermak Plateau (Fig. 1) (*16*). We have analyzed samples from four selected sediment cores from the Gakkel Ridge (core PS2163-1: 86.24°N, 59.22°E; water depth 3040 m; core PS2206-4: 84.28°N, 02.51°W; water depth 2993 m), the Amundsen Basin (core PS2170-4: 87.59°N, 60.77°E; water depth 4226 m), and the Lomonosov Ridge (core PS2177-3: 88.04°N, 134.93°E; water depth 1388 m). All four cores, including the basin core PS2170-4, which was cored on an isolated submarine high a few hundred meters above the abyssal plain to exclude turbidites, sampled undisturbed pelagic sediments (*16*). We determined stable isotope records, on planktonic foraminifera shells of *Neogloboquadrina pachyderma sin.* and benthic foraminifera shells of *Cibicidoides wuellerstorfi*, and carbonate and organic carbon (*17*).

On the basis of the AMS ^{14}C dates (Table 1) (*18*), the stable isotope records represent oxygen isotope stage 1, stage 2, and (the upper part of) stage 3 (Fig. 2). The records generally agree with a global isotope (climate) curve, at least in the upper part. The distinct decrease in ∂^{18}O (*19*) toward the tops of the cores represents the transition from the last glacial period to the Holocene interglacial period (Termination I) (*1, 5, 6, 20, 21*). In all four cores, this transition is a two-step change, which may correspond to Terminations Ia and Ib. The higher ∂^{18}O values between Terminations Ia and Ib may correspond to the Younger Dryas event (*22, 23*). Termination Ib is furthermore characterized by a distinct increase in contents of biogenic carbonate (foraminifers and coccoliths) and organic carbon (Fig. 2). The age control in the lower parts of the sedimentary records, especially core PS2163, is less precise because of the larger errors on the AMS ^{14}C dates.

In general, our AMS ^{14}C and isotope data indicate that sedimentation rates in the postglacial eastern central Arctic Ocean were 0.7 to about 1.0 cm per thousand years (Table 2), in contrast to rates of a few millimeters per thousand years for the western central Arctic Ocean (*11, 13*). Calculated sedimentation rates for the Holocene interval at AMS ^{14}C dated cores from the Gakkel Ridge were also similar (*10, 24*). Holocene sedimentation rates higher than ours have been determined on the basis of calcareous nannofossil stratigraphy from ARCTIC '91 cores (*14*). On the basis of the AMS ^{14}C dates, the sedimentation rates of the last glacial interval were about 0.5 cm per thousand years (Table 2).

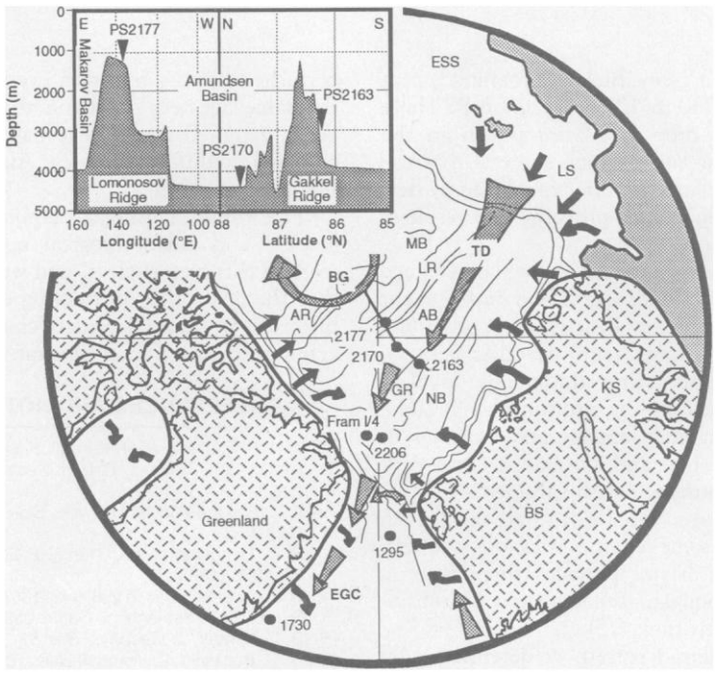

Fig. 1. Locations of cores (●) investigated and mentioned in the text. Hatched area indicates approximate limit of the Northern Hemisphere ice sheets during the last glacial maximum (*51*). Stippled arrows indicate surface-water circulation; small solid, arrows indicate supply of low-saline waters (meltwater); heavy line connecting dots mark the cross section shown in the inset. TD, Transpolar Drift; BG, Beaufort Gyre; EGC, East Greenland Current; ESS, East Siberian Sea; LS, Laptev Sea; KS, Kara Sea; BS, Barents Sea; NB, Nansen Basin; GR, Gakkel Ridge; AB, Amundsen Basin; LR, Lomonosov Ridge; MB, Makarov Basin; AR, Alpha Ridge.

R. Stein, S.-I. Nam, C. Schubert, C. Vogt, D. Fütterer, Alfred Wegener Institute for Polar and Marine Research, Columbusstrasse, 27568 Bremerhaven, Germany.
J. Heinemeier, Institute of Physics and Astronomy, University of Aarhus, 8000 Aarhus C, Denmark.

It is generally accepted that the oxygen isotopic composition of the planktonic foraminiferal species *N. pachyderma sin.* is in equilibrium with the isotopic composition of the surface water (*25*). In addition, the $\partial^{18}O$ values in the foraminiferal tests are strongly controlled by the seawater temperature (*20, 26*). In the central Arctic Ocean north of 83°N, *N. pachyderma sin.* lives in the surface mixed layer (50 to 100 m) (*27*), which is characterized by its rather constant, very low temperature close to the freezing point (around −1.7°C) (*28, 29*). The salinities, on the other hand, vary between about 30 and 33.5 per mil in the central Arctic Ocean; values decrease from the Nansen Basin (>33 per mil) toward the Lomonosov Ridge and Makarov Basin (<31.5 per mil) (*28, 29*). The salinity distribution in the central Arctic is mainly controlled by the river discharge and the transport of this low-saline water from the shelf areas to the open ocean by the Transpolar Drift system. In the modern central Arctic Ocean, about 10% of the water column is made up of river water (*30*). Thus, changes in the isotopic composition in the planktonic foraminiferal calcite tests from the central Arctic do not reflect changes in temperature. Instead, they indicate changes in the isotopic composition of the seawater, which is linearly related to the salinity (*31, 32*). This relation between modern surface-water salinity and oxygen stable isotopes of *N. pachyderma sin.* can be seen in Arctic Ocean surface sediments (including ARCTIC '91 samples) (*33*). The distinct general trend toward lighter oxygen isotope values from the Gakkel Ridge (core PS2163) toward the Amundsen Basin (core PS2170) and the Lomonosov Ridge (core PS2177) also supports this relation (Fig. 2).

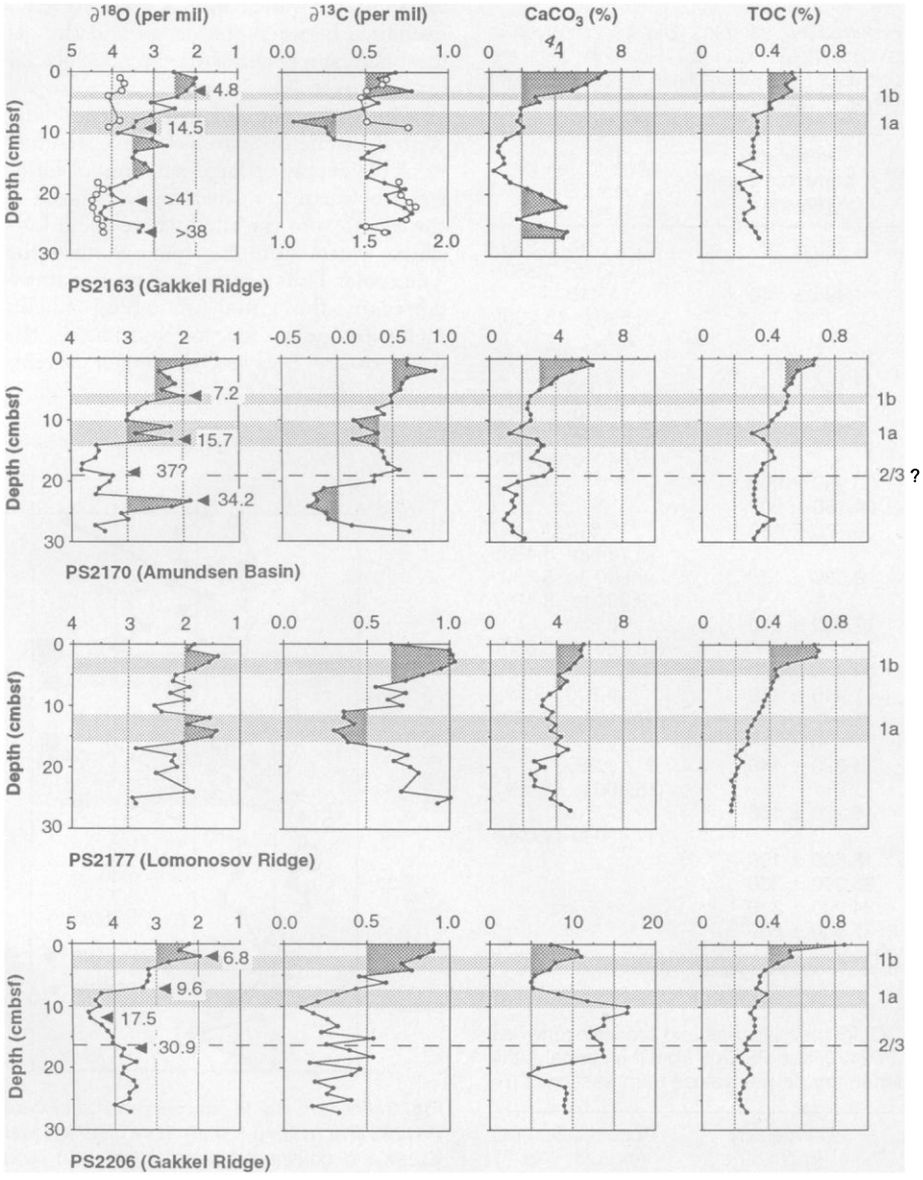

Fig. 2. Oxygen and carbon stable isotopes, determined on *N. pachyderma sin.*, and carbonate and total organic carbon (TOC) contents. At core PS2163, stable isotope values were also determined on *C. wuellerstorfi* (open circles); benthic carbon isotope values are given at the bottom of the diagram. Between 10 and 17 cm below sea floor (cmbsf), *C. wuellerstorfi* is absent in the sediments of core PS2163, suggesting that this interval may correspond to the last glacial interval. Numbers at the oxygen isotope records are reservoir-corrected AMS ^{14}C ages in thousands of years B.P. (Table 1). The AMS ^{14}C dates >38,000 years at core PS2163 are finite ages. The slight inversion at core PS2170 might be ascribed to small effects of reworking. Shaded horizontal bars indicate Termination Ia and Ib; dashed line indicates the oxygen isotope stage 2/3 boundary.

Comparing the isotope values from before the onset of Termination I with the surface (near-modern) ones, it is obvious that the glacial-interglacial differences in $\partial^{18}O$ are irregular among the four cores. They range between 2.4 per mil in core PS2206 at the western Gakkel Ridge and 1.6 to 1.2 per mil in cores PS2163, PS2170, and PS2177 at the eastern Gakkel Ridge, the Amundsen Basin, and the Lomonosov Ridge, respectively. A large glacial-interglacial shift in $\partial^{18}O$ of 2.7 per mil is also recorded at Fram Basin core FRAM-I/4, which is close to core PS2206 (Fig. 1) (*9*). At the western Gakkel Ridge, this difference distinctly exceeds the shift in $\partial^{18}O$ of about 1.3 per mil attributed to changes in the glacial-interglacial ice volume (*23, 34, 35*), but the differences are similar to the ice-volume signal in the central Arctic. Because the modern surface-water temperatures in the central Arctic Ocean are already low and close to the freezing point (*29*), a further cooling during glacial times is unrealistic. Thus, the excess in $\partial^{18}O$ at the western Gakkel Ridge was probably caused by a decrease in salinity resulting from increased meltwater discharge during the last deglaciation (Termination I). At Lomonosov Ridge, where the glacial-interglacial difference is closest to the ice-volume signal, the salinity of the last glacial surface waters was likely similar to the modern one, and the Transpolar Drift might have also transported significant quantities of low-salinity waters into the central Arctic Ocean during those glacial times. At the western Gakkel Ridge and in the Fram Basin, on the other hand, glacial salinity was probably significantly higher in comparison to today because the supply of meltwater was reduced then. On the basis of the comparison of modern salinity and temperatures of surface and bottom waters and oxygen isotope data from planktonic and benthic foraminifera of surface sediments from the central Arctic Ocean (*36*),

glacial surface waters were about 1.1 to 1.4 per mil more saline than waters today in the western Gakkel Ridge area.

The ^{14}C date at the beginning of the glacial-interglacial transition, indicated by a distinct, rapid $\partial^{18}O$ depletion of up to 1.4 per mil, is 15.7 thousand years ago (ka) (or 16,650 years B.C. in calendar years) (*18*) (Figs. 2 and 3; Table 1). This $\partial^{18}O$ shift is almost contemporaneous with a distinct $\partial^{13}C$ minimum, which can be correlated from the eastern Gakkel Ridge through the Amundsen Basin to the Lomonosov Ridge (Fig. 2). Both shifts can clearly be identified at all other cores from this area, including the Makarov Basin (*36*). These records suggest that there was a strong meltwater influx at the very beginning of Termination I. The thick meltwater cover probably resulted in a major widespread stratification and decrease in ventilation of near-surface waters, as reflected in the distinct $\partial^{13}C$ minima. A similar, older (stage 3?) influx of meltwater is probably represented in the isotope records of core PS2170 at a depth of about 25 cm below sea floor (cmbsf) (Fig. 2). During these events, carbonate productivity (mainly planktonic foraminifers) evidently decreased, indicated by distinctly reduced carbonate contents in the early stage 1 sediments (Fig. 2). The lack of distinct $\partial^{13}C$ and $\partial^{18}O$ minima at core PS2206 suggests that the meltwater pulse probably did not reach the western Gakkel Ridge during this early phase of deglaciation. The distinct $\partial^{13}C$ minimum at this core at about 10 cmbsf, which coincides with high $\partial^{18}O$ values, represents the uppermost stage 2 (Fig. 2) and was probably caused by a reduced oxygenation of near-surface waters and a reduced CO_2 exchange between the ocean and the atmosphere as a result of an extended glacial sea-ice cover (*9*).

This early influx of meltwater into the central Arctic Ocean may have resulted from the supply of large amounts of freshwater by the major Siberian rivers (such as the Lena) onto the shelf where these low-saline waters were incorporated into the Transpolar Drift system and further transported into the central Arctic (Fig. 1). This meltwater pulse appears to indicate the onset of the decay of the major Barents

Table 1. The AMS ^{14}C datings performed on *N. pachyderma sin.* samples. Depths are given in centimeters below the sea floor (cmbsf). The various ages (given with ±1 SD) and units are explained in (*18*). The AMS ^{14}C dates >38,000 years at core PS2163 are finite ages. The slight inversion at core PS2170 might be ascribed to small effects of reworking.

Core	Lab no.*	Depth (cmbsf)	Age (years B.P.)	Reservoir-corrected age (years B.P.)	Age (calendar years B.C.)
PS2163	AAR-1159	3.5	5,250 ± 80	4,750 ± 80	3,620 to 3,530 (3,640 to 3,380)
	AAR-1160	9.5	15,040 ± 140	14,490 ± 140	15,410 (15,590 to 15,230)
	AAR-1161	22.5	>41,000		
	AAR-1162	25.5	>38,000		
PS2170	AAR-1163	6.5	7,740 ± 90	7,190 ± 90	6,000 (6,120 to 5,960)
	AAR-1164	13.5	16,260 ± 180	15,710 ± 180	16,650 (16,840 to 16,470)
	AAR-1165	18.5	37,500 ± 900	36,950 ± 900	
	AAR-1166	23.5	34,700 ± 600	34,150 ± 600	
PS2206	AAR-1167	3.5	7,320 ± 180	6,770 ± 180	5,610 (5,760 to 5,450)
	AAR-1168	7.5	10,130 ± 120	9,580 ± 120	8,900 to 8,630 (9,000 to 8,470)
	AAR-1169	12.5	18,050 ± 340	17,500 ± 340	18,880 (19,360 to 18,350)
	AAR-1170	18.5	31,450 ± 550	30,900 ± 550	
PS1730	AAR-1152	43	8,460 ± 110	7,910 ± 110	6,700 (7,010 to 6,570)
	—	58	Vedde ash†	10,600	
	AAR-1153	93	14,870 ± 140	14,320 ± 140	15,220 (15,400 to 15,030)
	AAR-1154	103	16,820 ± 150	16,270 ± 150	17,210 (17,420 to 17,020)
	AAR-1155	113	19,150 ± 190	18,600 ± 190	
	AAR-1156	163	23,550 ± 360	23,000 ± 360	
	AAR-1157	183	24,540 ± 310	24,900 ± 310	
	AAR-1158	223	28,500 ± 650	27,950 ± 650	

*Number at AMS Laboratory, Aarhus University. †The age of the Vedde ash is given by Mangerud *et al.* (*52*).

Table 2. Accumulation rates of total organic carbon (TOC) for the Holocene and pre-Holocene (last glacial) intervals at the AMS ^{14}C-dated cores PS2163, PS2170, and PS2206 from the central Arctic Ocean. TOC is percent of the bulk sediment sample. Mean dry density values from Kassens (*16*).

Core	Sedimentation rate (cm ka^{-1})	TOC (%)	Dry density (g cm^{-3})	Accumulation rate (mg cm^{-2} ka^{-1})
PS2163				
Holocene	0.7	0.55	0.75	2.9
Last glacial	<0.7	0.3	0.75	<1.5
PS2170				
Holocene	0.85	0.7	0.75	4.5
Last glacial	0.5	0.4	0.75	1.5
PS2206				
Holocene	0.7	0.5	0.75	2.6
Last glacial	0.5	0.3	0.75	1.1

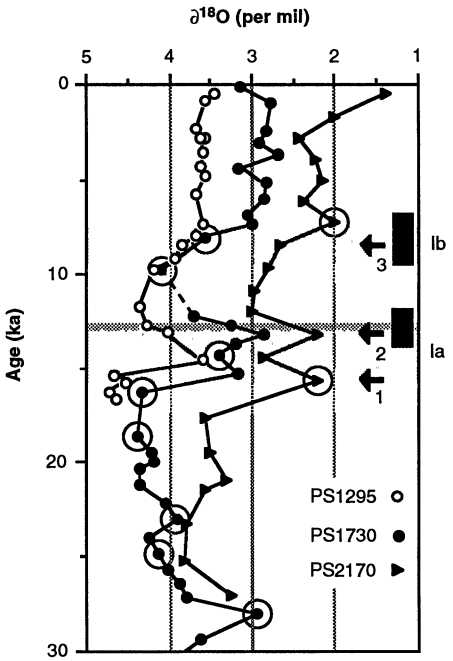

Fig. 3. Oxygen stable isotope records of core PS1295 (Fram Strait) (○) (*6*), core PS1730 (east Greenland continental margin) (●) (*40*), and core PS2170 (Amundsen Basin) (▶) versus age (with a reservoir correction of 550 years). Circled data points in the records of cores PS1730 and PS2170 are AMS ^{14}C-dated (Table 1); at core PS1295, all data points are AMS ^{14}C-dated. Shaded horizontal bars indicate Termination Ia and Ib; vertical black bars indicate the two major global meltwater events (*23*); and black arrows 1 through 3 indicate major meltwater pulses in the central Arctic Ocean.

Shelf (Eurasian Arctic) Ice Sheet during this early phase of deglaciation. If so, the increase in the supply of meltwaters from Siberian rivers began slightly before the major meltwater discharge recorded at Fram Strait core PS1295, which has been AMS ^{14}C-dated to about 14.5 ka (Figs. 1 and 3) (6).

The early Arctic Ocean meltwater signal clearly precedes major meltwater events recorded on the southeast Baffin shelf and the northernmost Labrador shelf (*37*) that correlate with pulses of global ice-sheet melting pulses at about 13.5 and 9 ka (*23, 35*). The two younger meltwater signals recorded at core PS2170 coincide with these two global pulses (Fig. 3). At those times, the rapid retreat of the Laurentide Ice Sheet also may have supplied major amounts of meltwater into the Arctic Ocean (*38, 39*).

All three central Arctic Ocean meltwater signals can also be identified at core PS1730, which is located at the east Greenland continental margin off Scoresby Sound (Fig. 1), one of the largest fjord systems of the world. This isotope record may reflect either the fluctuation of the Greenland Ice Sheet or changes in the flux of low-saline waters in the East Greenland Current system (Figs. 1 and 3) (*40*). Thus, the almost parallel trends of the oxygen isotope records shown in Fig. 3 may be indicative of contemporaneous variations of the Barents Sea and Greenland ice sheets. They might also signal, however, an increased export of low-saline waters from the Arctic within the East Greenland Current controlled by the decay of the Barents Sea and (for the two younger meltwater signals) Laurentide ice sheets. An early beginning of the decay of the Barents Sea Ice Sheet (represented in the Arctic Ocean and Fram Strait stable isotope records) and the Greenland Ice Sheet may have triggered the subsequent major decay of the Laurentide Ice Sheet (*37*) and the major retreat of glaciers from the western margin of Spitsbergen (*41, 42*), starting at about 13.5 to 12.5 ka (6). Furthermore, the influx of meltwater from the Arctic Ocean into the North Atlantic controlled by the decay of the major Northern Hemisphere ice sheets might have been critical for the North Atlantic deep water formation and, thus, important for global climate system changes (*43–45*).

During Termination Ib, ∂^{13}C values in the cores distinctly increased, as did carbonate and organic carbon concentrations (Fig. 2). The Holocene increase in ∂^{13}C to modern values recorded in most of the cores suggests that a well-oxygenated surface-water mass was extensive and more open-ice conditions prevailed in the Arctic Ocean at the end of Termination I. Because the carbonate material is mainly composed of planktonic foraminifera, coccoliths and ostracodes (*14, 46*) and changes in carbonate dissolution can be neglected at depths less than 4500 m (*47*), the reduced sea-ice cover and at least seasonally open waters may have increased surface-water productivity (*14*). The organic carbon levels are probably not a pure productivity signal because major proportions of the organic matter are of terrigenous origin (*48, 49*). The glacial-to-interglacial increase in accumulation rates of total organic carbon by a factor of 2 or 3 (Table 2) was thus mainly caused by an increased supply of terrigenous organic matter from Eurasia. The flux of marine organic matter may also have increased during the Holocene, but oxic, well-ventilated deep-water conditions [inferred from the homogenous brown sediments (*16*) and high ∂^{13}C values determined from C. *wuellerstorfi* tests] and low sedimentation rates would have precluded its preservation.

By the end of Termination Ib (about 7.2 ka or 6000 calendar years B.C.), the maximum (modern) difference between ∂^{18}O values of planktonic and benthic foraminifera was reached (Fig. 2, core PS2163), suggesting that the modern characteristics of the surface- and deep-water masses have existed since that time. The distinctly reduced difference in the planktonic and benthic oxygen stable isotope values recorded at core PS2163 in the lower part of the sedimentary sequence, on the other hand, indicates that (if major temperature changes are neglected) the salinity difference between the surface water layer and the deeper water masses was probably smaller than it is today, and the strong vertical stratification of the modern Arctic Ocean should have been less pronounced during this earlier (stage 3?) time interval.

REFERENCES AND NOTES

1. J.-C. Duplessy *et al.*, *Nature* **320**, 350 (1986).
2. R. H. Fillon and D. F. Williams, *ibid.* **310**, 674 (1984).
3. E. Bard and W. S. Broecker, Eds., *The Last Deglaciation: Absolute and Radiocarbon Chronologies* (NATO ASI Series 12, Springer-Verlag, New York, 1992).
4. W. F. Ruddiman and H. E. Wright Jr., Eds., *North America and Adjacent Oceans During the Last Deglaciation*, vol. K-3 of *The Geology of North America* (Geological Society of America, Boulder, CO, 1987).
5. E. Jansen and T. Veum, *Nature* **343**, 612 (1990).
6. G. A. Jones and L. D. Keigwin, *ibid.* **336**, 56 (1988).
7. M. Sarnthein *et al.*, in (*3*), pp. 183–200.
8. A. E. Aksu, *Geol. Surv. Can. Pap. 84-22* (1985), p. 115.
9. R. Zahn, B. Markussen, J. Thiede, *Nature* **314**, 433 (1985).
10. S. E. I. Köhler, *GEOMAR Rep. 13* (Kiel University, Kiel, Germany, 1992).
11. D. L. Clark, R. R. Whitman, K. A. Morgan, S. D. Mackay, *Geol. Soc. Am. Spec. Pap. 181* (1980).
12. H. P. Sejrup, G. H. Miller, J. Brigham-Grette, R. Lovlie, D. Hopkins, *Nature* **310**, 772 (1984).
13. S. A. Macko and A. E. Aksu, *ibid.* **322**, 730 (1986).
14. G. Gard, *Geology* **21**, 227 (1993).
15. Y. Herman, Ed., *The Arctic Seas* (Van Nostrand Reinhold, New York, 1989).
16. D. K. Fütterer, *Ber. Polarsternforschung* **107**, 267 (1992).
17. All four cores were sampled every centimeter. For stable isotope measurements, 10 specimens of the planktonic foraminifera *N. pachyderma sin.* of the 125- to 250-μm fraction and two to three specimens of the benthic foraminifera *C. wuellerstorfi* were used for each analysis. Measurements were performed on a Finnigan MAT 251 mass spectrometer, following standard procedures. Total carbon and organic carbon were determined on ground bulk samples and carbonate-free sediment samples, respectively, by means of a CHN elemental analyzer. For AMS ^{14}C dating, about 2000 specimens of *N. pachyderma sin.* were picked for each analysis; the dating was performed at the AMS ^{14}C Dating Laboratory of the Institute of Physics and Astronomy, Aarhus University, Denmark.
18. The ^{14}C ages are given in conventional radiocarbon years B.P. (before present, 1950 A.D.). Dates of marine samples (for example, foraminiferal tests) have to be corrected for reservoir effects to be comparable with contemporaneous terrestrial material. The reservoir effect (about 550 years) is subtracted from the conventional ^{14}C age to obtain reservoir-corrected ages. Reservoir-corrected ^{14}C ages [in thousands of years B.P. (ka)] are presented in the text and Figs. 2 and 3. In addition, calibrated ages in calendar years B.C. have been obtained from calibration tables by means of the Seattle calibration program, version 3.0 (*50*). The intercept with the calibration curve is given (as an interval if more than one intercept). The intercept method has been used to calculate the calibrated age interval corresponding to ±1 standard deviation in the conventional ^{14}C age.
19. The isotope values are recorded relative to the Pee Dee belemnite (PDB) standard in the ∂ notation, where $\partial = [(R_{sample}/R_{standard}) - 1] \times 1000$ and $R = {}^{18}O/{}^{16}O$ or ${}^{13}C/{}^{12}C$. The results are expressed in per mil.
20. E. Bard *et al.*, in *Geological History of the Polar Oceans: Arctic Versus Antarctic*, U. Bleil and J. Thiede, Eds. (Kluwer, Dordrecht, Netherlands, 1990), pp. 405–415.
21. W. F. Ruddiman and J.-C. Duplessy, *Quat. Res.* **23**, 1 (1985).
22. J.-C. Duplessy, G. Delibrias, J. L. Turon, C. Pujol, J. Duprat, *Palaeogeogr. Palaeoclimatol. Palaeoecol.* **35**, 121 (1981).
23. R. G. Fairbanks, *Nature* **342**, 637 (1989).
24. J. Mienert, L. A. Mayer, A. Jones, J. W. King, in (*20*), pp. 455–474.
25. C. D. Charles and R. G. Fairbanks, *ibid.*, pp. 519–538.
26. S. Epstein, R. Buchsbaum, H. A. Lowenstam, H. C. Urey, *Geol. Soc. Am. Bull.* **64**, 1315 (1953).
27. J. Carstens and G. Wefer, *Deep-Sea Res.* **39** (no. 2), S507 (1992).
28. S. G. Gorshkov, Ed., *World Ocean Atlas: Arctic Ocean, Vol. 3* (Pergamon, Oxford, 1983).
29. L. G. Anderson *et al.*, *J. Geophys. Res.* **99**, 3273 (1993).
30. G. Östlund, "Transport pattern of Siberian river water in the Arctic Basin" (Workshop report, Kirkenes, Norway, 1993).
31. H. Craig and L. I. Gordon, in *Symposium Proceedings Marine Chemistry*, D. Schink and B. H. Corliss (University of Rhode Island, Kingston, RI, 1965), pp. 277–374.
32. R. G. Fairbanks, C. D. Charles, J. D. Wright, in *Radiocarbon After Four Decades*, R. E. Taylor, Ed. (Springer Verlag, New York, 1992), pp. 473–500.
33. R. F. Spielhagen and E. Erlenkeuser, *Mar. Geol.*, in press.
34. J. Chappell and N. J. Shackleton, *Nature* **324**, 137 (1986).
35. W. F. Ruddiman, in (*4*), pp. 463–478.
36. R. Stein, C. Schubert, C. Vogt, D. Fütterer, *Mar. Geol.*, in press.
37. J. T. Andrews, H. Erlenkeuser, L. W. Evans, W. M. Briggs, A. J. T. Jull, *Paleoceanography* **6**, 621 (1991).
38. A. S. Dyke and V. K. Prest, *Géogr. Phys. Quat.* **41**, 237 (1987).

39. J. T. Andrews, A. S. Dyke, K. Tedesco, J. W. White, *Geology* **21**, 881 (1993).
40. S.-I. Nam, R. Stein, H. Grobe, H. Hubberten, in preparation.
41. J. Mangerud *et al.*, *Quat. Res.* **38**, 1 (1992).
42. J. I. Svenden, J. Mangerud, A. Elverhoi, A. Solheim, R. T. E. Schüttenhelm, *Mar. Geol.* **104**, 1 (1992).
43. R. R. Dickenson, J. Meincke, S. Malmberg, A. Lee, *Prog. Oceanogr.* **20**, 103 (1988).
44. W. S. Broecker and G. H. Denton, *Geochim. Cosmochim. Acta* **53**, 2465 (1989).
45. T. F. Stocker, D. G. Wright, W. S. Broecker, *Paleoceanography* **7**, 529 (1992).
46. T. M. Cronin, T. R. Holtz Jr., R. C. Whatley, *Mar. Geol.*, in press.
47. U. Pagels, *GEOMAR Rep. 10* (Kiel University, Kiel, Germany, 1991).
48. R. Stein, C. Schubert, H. Grobe, D. Fütterer, in *Proceedings of the 1992 International Conference on Arctic Margins*, D. K. Thurston, Ed. (Alaska Geological Society, Anchorage, AK, in press).
49. R. Stein, H. Grobe, M. Wahsner, *Mar. Geol.*, in press.
50. M. Stuiver and P. J. Reimer, *Radiocarbon* **35**, 215 (1993).
51. CLIMAP, *Map and Chart Ser. MC-36* (Geological Society of America, Boulder, CO, 1981).
52. J. Mangerud, S. E. Lie, H. Furnes, I. L. Kristiansen, *Quat. Res.* **21**, 85 (1984).
53. We thank the captain and the crew of the *R.V. Polarstern* for cooperation during the ARCTIC '91 expedition and two anonymous reviewers for their numerous helpful comments. Supported by the Deutsche Forschungsgemeinschaft (grant STE 412/6). Contribution 748 of the Alfred Wegener Institute for Polar and Marine Research.

20 December 1993; accepted 17 March 1994

Engineering Cell Shape and Function

Rahul Singhvi, Amit Kumar, Gabriel P. Lopez, Gregory N. Stephanopoulos, Daniel I. C. Wang, George M. Whitesides,* Donald E. Ingber*

An elastomeric stamp, containing defined features on the micrometer scale, was used to imprint gold surfaces with specific patterns of self-assembled monolayers of alkanethiols and, thereby, to create islands of defined shape and size that support extracellular matrix protein adsorption and cell attachment. Through this technique, it was possible to place cells in predetermined locations and arrays, separated by defined distances, and to dictate their shape. Limiting the degree of cell extension provided control over cell growth and protein secretion. This method is experimentally simple and highly adaptable. It should be useful for applications in biotechnology that require analysis of individual cells cultured at high density or repeated access to cells placed in specified locations.

New approaches to drug screening, in vitro toxicology, and genetic engineering focus on the analysis of functional changes within individual cultured cells (*1*). While potentially exciting, these approaches are limited in that cell shape and, hence cell behavior (*2–7*) can vary greatly from cell to cell within the same population in a culture dish. Further, it is difficult to analyze many randomly oriented cells simultaneously or to return to the same cell after measurements have been made in other locations. Thus, a convenient method for physically isolating large numbers of individual cells cultured at high density, controlling their shape, and reproducibly defining their distribution would be extremely valuable.

We now report a simple and flexible method for the construction of tissue culture substrata that contain adhesive islands distributed in defined sizes, shapes, and patterns (Fig. 1) and demonstrate their utility for controlling cell shape, growth, and function. An elastomeric polydimethylsiloxane (PDMS) stamp was used to pattern the adsorption of a hexadecanethiol [$HS(CH_2)_{15}CH_3$] in a self-assembled monolayer (SAM) on gold substrata (Fig. 1A) (*8, 9*). The remaining bare gold regions were derivatized with a polyethylene glycol (PEG)–terminated alkanethiol [$HS(CH_2)_{11}(OCH_2CH_2)_6OH$]; SAMs of this alkanethiolate resist adsorption of proteins (*10*). Through this technique, hexadecanethiolate regions of defined size (lateral dimensions of 2 to 80 μm) that supported protein adsorption were produced on otherwise nonadhesive gold surfaces (Fig. 1B). The exposure of this substratum to the purified extracellular matrix (ECM) protein, laminin, resulted in the formation of protein-coated islands of defined geometry and distribution (Fig. 1C) that corresponded precisely to the patterns formed from SAMs of hexadecanethiolate (Fig. 1B).

The ability of this technique to control cell distribution and shape was explored by the plating of primary rat hepatocytes in hormonally defined medium (*7*) on laminin-coated substrata that were stamped with square and rectangular islands having micrometer-scale dimensions (*9*). Cells attached preferentially to the adhesive, lami-

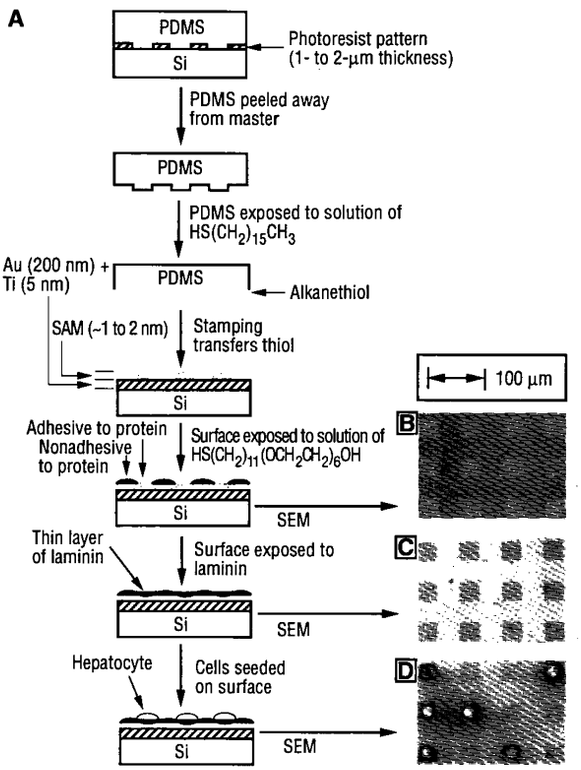

Fig. 1. (**A**) Diagrammatic representation of the method for the fabrication of the rubber stamp and the creation of patterned substrata (*8, 9*). (**B**) Scanning electron micrograph of the substrate after the imprinting of 40 μm by 40 μm squares with hexadecanethiol [$HS(CH_2)_{15}CH_3$] and exposure to PEG-terminated alkanethiol [$HS(CH_2)_{11}(OCH_2CH_2)_6OH$, PEG-thiol]. Adhesive hexadecanethiolate-coated regions appeared light against a darker, nonadhesive background coated with PEG-thiolate, as reported (*18*). (**C**) Scanning electron micrograph of a laminin-coated patterned substratum. Protein coating resulted in a reversal of the light and dark staining patterns (*18*). (**D**) Scanning electron micrograph of a similar laminin-coated substratum containing adherent rat hepatocytes.

R. Singhvi, G. N. Stephanopoulos, D. I. C. Wang, Biotechnology Processing Engineering Center and Department of Chemical Engineering, Massachusetts Institute of Technology, Cambridge, MA 02139, USA.
A. Kumar, G. P. Lopez, G. M. Whitesides, Department of Chemistry, Harvard University, Cambridge, MA 02138, USA.
D. E. Ingber, Departments of Surgery and Pathology, Children's Hospital, and Harvard Medical School, Enders 1007, 300 Longwood Avenue, Boston, MA 02115, USA.
*To whom correspondence should be addressed.